

Self-limit in glaser crystallization and direct writing of 2D materials

¹pradyumna Kumar Pradhan, ²soubhagini Mandal,

*Gandhi Institute of Excellent Technocrats, Bhubaneswar, India
Black Diamond College of Engineering & Technology, Jharsuguda, Odisha, India*

ABSTRACT:

Direct growth and patterning of atomically thin two-dimensional (2D) materials on various substrates are essential steps towards enabling their potential for use in the next generation of electronic and optoelectronic devices. The conventional gas-phase growth techniques, however, are not compatible with direct patterning processes. Similarly, the condensed-phase methods, based on metal oxide deposition and chalcogenization processes, require lengthy processing times and high temperatures. Here, a novel self-limiting laser crystallization process for direct crystallization and patterning of 2D materials is demonstrated. It takes advantage of significant differences between the optical properties of the amorphous and crystalline phases. Pulsed laser deposition is used to deposit a thin layer of stoichiometric amorphous molybdenum disulfide (MoS₂) film (~ 3nm) onto the fused silica substrates. A tunable nanosecond infrared (IR) laser (1064nm) is the employed to couple a precise amount of power and number of pulses into the amorphous materials for controlled crystallization and direct writing processes. The IR laser interaction with the amorphous layer results in fast heating, crystallization, and/or evaporation of the materials within a narrow processing window. However, reduction of the midgap and defect states in the as-crystallized layers decreases the laser coupling efficiency leading to higher tolerance to process parameters. The deliberate design of such laser-2D material interactions allows these self-limiting crystallization phenomena to occur with increased quality and a much broader processing window. This unique laser processing approach allows high-quality crystallization, direct writing, patterning, and the integration of various 2D materials into future functional devices.

Keywords: 2D materials, direct laser writing, laser crystallization
(Some figures may appear in colour only in the online journal)

INTRODUCTION

The recent discovery of atomically thin two-dimensional (2D) materials has revealed promising potential for advancing the future of optoelectronics, photonics, sensing, and energy applications [1–19]. In particular, mono- and few-layer transition metal dichalcogenides (TMDCs) with a general formula of MX₂ (where M=Mo, W, etc; X=S, Te, Se) have attracted significant research attention motivated primarily by their exciting electronic, optical, and photonic properties in the visible and near-infrared part of the spectrum [20–23]. For instance, some of these materials (e.g. WS₂, MoS₂, MoSe₂, WSe₂) transition from an indirect to direct [24, 25] bandgap as they reach a single-layer limit. Due to their reduced screening of Coulomb interactions, TMDCs exhibit strong many-body interactions which result in strong binding of excitons, biexcitons [26], and trions [27]. Broken inversion symmetry and strong spin-orbit coupling [28] can also open the possibility for nonlinear light-matter interactions, including second harmonic generation in these materials.

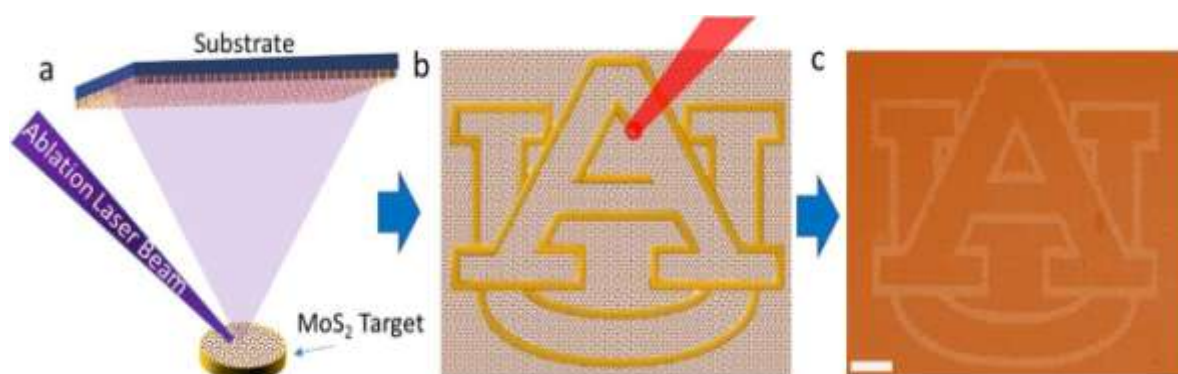


Figure 1. Schematic representations of the experimental design and process flow. Pulsed laser deposition (a) and laser writing/crystallization setups (b) were used for deposition of amorphous thin films and crystallization/writing of 2D materials, respectively. The optical image (c) shows a representative laser-crystallized MoS_2 pattern (Auburn University logo) on the fused silica substrate. The bright lines and dark background indicate the crystalline and amorphous regions, respectively. The scale bar is $200\mu\text{m}$.

A significant amount of research interest has been devoted to scalable, tunable, and defect-free synthesis and processing of TMDCs [29–35]. Many synthesis techniques, including chemical vapor deposition [36], metalorganic chemical vapor deposition [37], and molecular beam epitaxy (MBE) [38], have been developed to control the growth of such materials on various substrates. Despite significant progress in the growth of a few 2D TMDCs using these techniques, they have major disadvantages when it comes to device integration and patterning flexibility. For instance, very high substrate temperatures (e.g. 850°C) in the above-mentioned growth methods significantly limit their compatibility with flexible or traditional semiconductor patterning and device integration technologies (e.g. photolithography). In order to overcome these major issues, novel synthesis and processing approaches are required.

Here, a laser-based synthesis and processing method is reported that relies on self-limiting laser crystallization (SLC) of stoichiometric amorphous thin films ($\sim 3\text{--}5\text{ nm}$) deposited on fused silica substrates via pulsed laser deposition (PLD) of a MoS_2 target. This technique mainly takes advantage of significant contrasts between the optical properties of the amorphous and crystalline MoS_2 phases. MoS_2 was chosen as the material of interest due to its fast crystallization process with no further effect on the irradiated/crystallized materials leading to a higher tolerance to process parameters, better crystallinity, and a much broader process window.

1. Experimental design

Figure 1 shows the schematics of our laser synthesis and processing approaches with a representative optical image showing a laser-crystallized, few-layer MoS_2 film on a fused silica substrate. In this process, we first deposited a thin film of stoichiometric amorphous 2D TMDCs on the fused silica substrates due to their high transparency at near-infrared (IR) (i.e. 1064 nm) wavelengths. This allowed us to minimize the laser interaction with the substrate during the crystallization process. PLD [33, 39, 40] was used as a versatile method of depositing a stoichiometric layer of MoS_2 thin film onto the substrate at room temperature. A 1-inch diameter MoS_2 target was placed on a target carousel inside a spherical chamber (21 inches in diameter). An excimer laser (COMPexPro[®], KrF248 nm, 20 ns) was used to ablate the MoS_2 target at a 40° angle of incidence and 2 Hz repetition rate. The resultant laser spot size and fluence on the target were $2\times 5\text{ mm}$ and

nating optoelectronic properties and the existence of a large amount of available data for validation of the results.

In general, a monolayer MoS₂ crystal is a direct bandgap of ~ 2 eV (620 nm) semiconductor [24]. However, when the film thickness is more than five layers, MoS₂ behaves like an indirect bandgap semiconductor with a smaller bandgap

1.3 eV (~ 950 nm) [24]. We show that a large number of the defect, imperfection, and midgap states in the amorphous materials enhance the absorption at below bandgap energies. The controlled irradiation of such amorphous materials with a tunable nanosecond 1064 nm laser offers multiple advantages by: (1) efficiently coupling into the amorphous film to selectively heat the materials, rearrange the atoms, and crystallize the films; (2) subsequently reducing the defects state and recovering the bandgap to its crystalline form; and

(3) reducing the coupling efficiency and self-limiting the

1.5 J cm⁻², respectively. The vacuum chamber was pumped down to 5×10^{-6} Torr for deposition, and the substrate-to-target distance was set at 13 cm. The number of deposition

pulses was kept at 200 for all of the depositions described in this paper for consistency.

After deposition of the amorphous MoS₂ thin films onto the fused silica substrates, we transferred the samples to a home-built environmental chamber for laser processing through a quartz window. The SLIC process and laser writing experiments were performed in an argon environment at atmospheric pressure and room temperature. The chamber was first flushed with argon gas for a few minutes to ensure the removal of possible oxygen residues followed by a 100 sccm flow rate to prevent air from entering into the chamber. Samples were then controllably crystallized by a 130 W tunable nanosecond laser capable of emitting

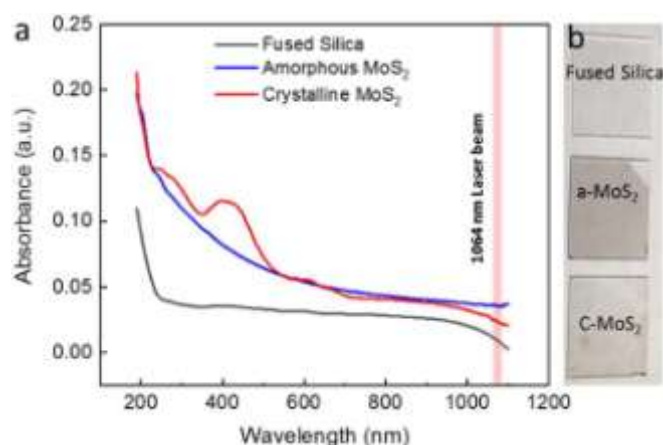


Figure 2. Absorption spectra (a) of fused silica (black), amorphous (blue), and crystalline (red) MoS₂ thin film. The spectra were taken from the samples in (b), as labeled. The crystallized sample shows absorption peaks at 680, 620, and 450 nm similar to the few-layer MoS₂ crystal [24]. The amorphous film shows higher absorption at 1064 nm than its crystalline counterpart.

nanosecond pulses (5–2000 ns in 63 waveforms) with a pulse energy from 0.04 to 1.57 mJ and a repetition rate ranging from 1 Hz to 4160 KHz. The laser beam was coupled into a galvo scanner with a 10 μ m focal point and a scan speed ranging from 1 to 5000 mm s⁻¹. A laser marking software (Laser Studio Professional) was used to design various patterns and control the process parameters (e.g. power, pulse duration, number of pulses, scan speed, repetition rate) for each specific pattern. We designed 5 \times 5 dot matrices with a 100 μ m distance between the dots throughout the experiments. The pulse width and repetition rate of the laser were kept constant at 261 ns and 1 MHz, respectively, in all of the experiments.

2. Results and discussions

To establish the SLIC concept, we first studied the absorption behavior of the MoS₂ thin films deposited, both before and after the crystallization process. According to the absorption spectra shown in figure 2, the crystallized MoS₂ samples developed clear peaks at 680 and 620 nm similar to the absorption peaks of mono- and few-layer MoS₂ crystals [24]. The absorption spectrum of amorphous MoS₂ thin film, on the other hand, did not show any identifiable peak. However, the amorphous film showed higher absorption at near-

IR (e.g. 1064 nm), nearly twice as large as its crystalline counterpart. The lack of distinct absorption peaks in amorphous MoS₂ films can be attributed to a large number of defect, imperfection, and midgap states [41] in the material that are also responsible for their enhanced absorption at below bandgap wavelengths.

Taking the optical absorption data into consideration, we studied the interaction of a 1064 nm tunable nanosecond laser beam with the amorphous MoS₂ film. We found that the laser interaction with the amorphous material often resulted in the evaporation of the 2D material with a very narrow choice of power and pulse numbers for crystallization. In the SLLC process, the crystallization was initiated at a low laser irradiation power (below the initial damage threshold); and once the amorphous MoS₂ film started to crystallize, the light interaction with the material became weaker due to the reduction of midgap and defect states in the crystallized structures. This initial crystallization and reduction in midgap states enabled us to significantly extend the laser power and pulse number far beyond the damage threshold to further improve the crystallization quality without damaging the MoS₂ layers.

In order to study the crystallization dynamics and identify the damage thresholds, we performed a systematic experimental study to find all of the possible noninteracting, crystallizing, and damaging zones as a function of laser power (from 65 to 130 W) and the number of pulses (from 2 to 50). Figures 3(a)–

(d) show the optical images of a set of patterns, on ~3 nm thick, PLD-deposited amorphous MoS₂ films created by various laser parameters, as indicated on the images. We performed a comprehensive experimental study to find how the material responds to the process parameters. We observed that the amorphous material was either unchanged, crystallized, or evaporated, depending on the laser power and the number of incident pulses. Generally, the effect of laser power and number of pulses was observed to be inversely proportional, i.e. increasing the laser power required the number of pulses to be decreased to induce the same effect

on the films. Figure 3(e) shows the heatmap of the zones experimentally obtained in this study. It was observed that the crystallization zone (red), where the best quality crystal form, was very narrow. Above this red zone, material damage (pink) and evaporation (white) occurred; and below it, crystallization quality faded (yellow) or no effect (blue) took place at all. As is apparent from the narrow crystallization window, high laser powers evaporated the materials due to the strong interaction with the amorphous film. To probe the structural evolution of the MoS₂ film in each zone, we performed a Raman study, as shown in figure 3(f). The Raman spectra and maps were acquired using a 532 nm laser excitation source, 50x objective lens, and 1200 lmm⁻¹ grating. The Raman spectra of amorphous films (Line 1) showed a broad shape with no visible peaks. The MoS₂ Raman fingerprints at 375 and 403 cm⁻¹ started appearing (Line 2) and getting stronger (Lines 3 and 4) for higher laser powers or number of pulses in the crystallization zone. Finally, the MoS₂ Raman peaks started disappearing (Line 5) as the process parameters entered the evaporation zone. Such a narrow crystallization zone limited the MoS₂ tolerance to even a small variation in the process parameters.

In principle, when the amorphous material is irradiated with a laser pulse, its temperature rises instantly. At high transient temperatures, the material gets close to its melting point which possesses different optical properties than at its crystalline phase. Therefore, further addition of energy into the system drives the material into the evaporation zone. To impose an SLLC condition, it is essential to design a multi-step processing sequence. We mainly started the SLLC process from a safe processing zone where the crystallization had

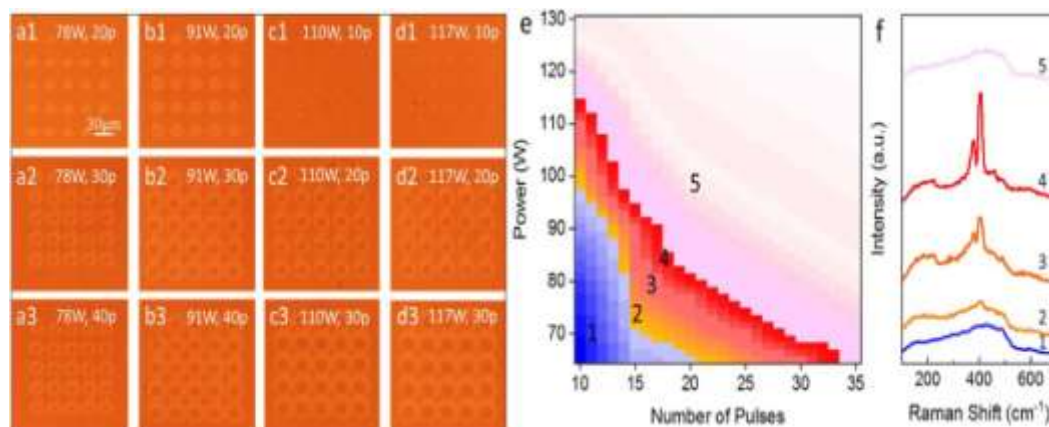


Figure 3. Representative optical images (a)–(d) and comprehensive heatmap (e) of the material's response to different laser powers and number of pulses. Blue, red, and pink zones are the process regions where no effect, crystallization, or damage occurred, respectively. The corresponding Raman spectra (f) show the structural evolution of the films in each region, as labeled.

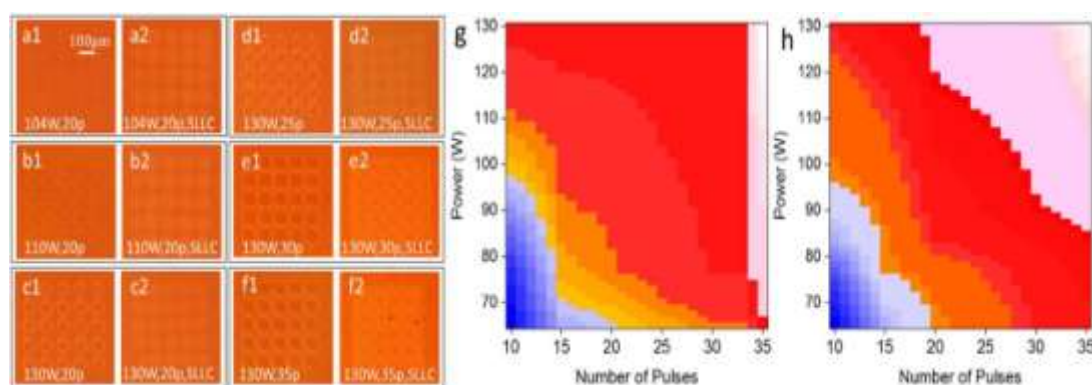


Figure 4. Representative optical images (a)–(f) showing the laser interaction effects on the amorphous MoS₂ film with and without the SLLC concept as labeled. Samples prepared using the SLLC approach were all crystallized without any visible damage, while all of their normally processed counterparts were evaporated. As shown, the self-limiting process can extend the safe crystallization zone up to 100% laser power without damage. Heatmaps show the broader crystallization zones (red) by either sequential powers sweep (g) or sequential pulse numbers sweep (h) during the crystallization process.

just been initiated (defined in figure 3(b)), followed by a sequential increase in the process parameters (i.e. laser power and/or pulse number) with a few milliseconds delay time between the process steps, allowing fast temperature quenching and crystal formation. This guided the material to its crystalline phase in each laser treatment, before pumping more energy into the material system.

Figures 4(a)–(f) show the representative optical images of MoS₂ thin film processed with and without the SLLC method. The images with a 1 following a letter represent the effect of laser power and the number of pulses that resulted in significant damage and evaporation in the normal laser processing approach, as indicated in figure 3. The images with a 2 following a letter show the perfectly crystallized samples prepared by the self-limiting process with no damage at all. For example, while the 104 W laser power with 20 pulses (figure 4(a1)) significantly damaged the film in the normal process, the SLLC approach did not damage the film even at 130 W (figure 4(f2)) where the laser power was increased from 65 to 130 W with a 1 W increment in laser power and 35 pulses in each step. To investigate this effect further, we performed a large set of experiments to identify noninteracting, crystallizing, and damaging process parameter zones in this sequential self-limiting process. Heatmaps of the material's response to sequential power (figure 4(g)) and pulse number increases (figure 4(h)) were plotted to visualize the resulting broad crystallization zones (red) in this process.

For sequential sweeping of power, the laser power was increased starting from 65 W to the desired power in 1 W incremental steps and a few milliseconds delay time between the steps, with a constant number of pulses in each step.

For sequential sweeping of the pulse number, the number of pulses was increased from 5 to 5 (where m ranges from 1 to 10) with a few milliseconds delay time between the steps and a constant power at each step. The blue color on the heatmap represents the unaffected zone, while the pink to white color indicates the decomposition and/or evaporation zones. It is evident from the heatmaps in figures 4(g) and (h) that better and broader crystallization zones (red) occurred in this method. This SLLC method significantly increased the process window as well as the quality of the MoS₂ crystals since the laser interacted with a 'crystalline' phase in each step (after the first treatment). Future modeling and theoretical

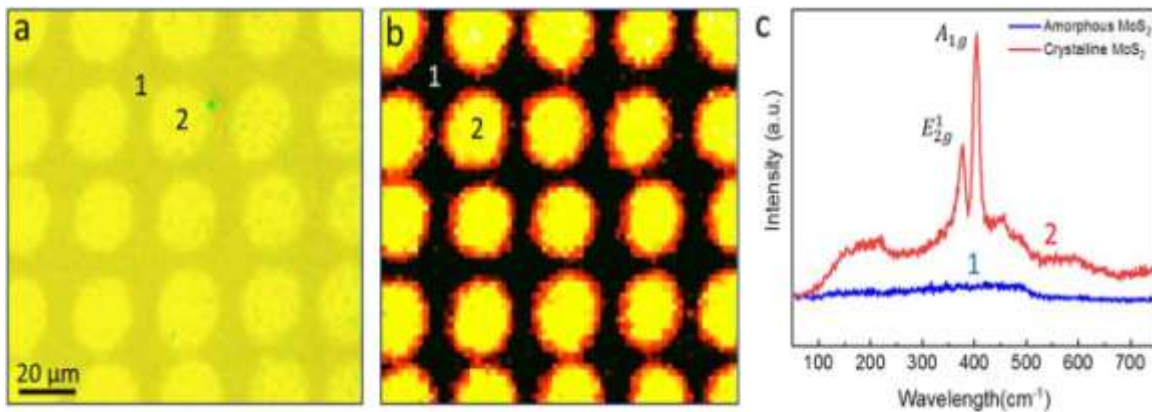


Figure 5. An optical image (a) and a Raman map (b) of a crystallized MoS₂ matrix showing the spatial uniformity of the crystalline regions. This sample was prepared in an SLLC approach by sweeping the power from 60 to 91 W with 1 W power increment and 30 pulses in each step. Raman spectra (c) obtained from the amorphous and crystallized regions as labeled on the images. The amorphous spectrum does not have any identifiable MoS₂ fingerprints while the crystallized part shows two intense peaks at 375 and 403 cm⁻¹ corresponding to crystalline MoS₂ materials.

work will be pursued to better understand the process kinetics.

Raman spectroscopy and mapping were carried out to probe the structural quality of the crystallized MoS₂ thin films. Figure 5(a) shows an optical image of a 5 × 5 crystalline MoS₂ matrix prepared by 91 W laser power and 30 laser pulses using the SLLC process. The corresponding Raman map of the matrix, figure 5(b), was plotted for the E_{2g}¹ mode of MoS₂ at 403 cm⁻¹. The uniform distribution of the Raman intensity in the map indicated the spatial uniformity of the crystallized MoS₂ dots. Representative Raman spectra of the sample from the amorphous and crystallized parts were also obtained, as shown in figure 5(c), indicating intense E_{2g}¹ and A_{1g} Raman peaks of MoS₂, similar to the results reported in the literature [42].

2g

CONCLUSION

In summary, we presented a novel SLLC approach by taking advantage of significant contrasts in the optical properties of amorphous and crystalline MoS₂ phases. We showed that the approach could extend the crystallization process zone and damage threshold well beyond the normal laser crystallization processes. A large number of defects, imperfections, and mid-gap states in the amorphous film enhanced the absorption at below bandgap energies. We showed that a tunable nano-second (1064 nm) laser could be efficiently coupled into such amorphous films to precisely heat the material, rearrange the atoms, and crystallize the film. Subsequently, due to appreciable changes in the absorption properties of MoS₂ as it crystallized, the laser energy coupling efficiency dropped, leading to a self-limiting crystallization process with no further effect on the irradiated/crystallized materials. We showed that the deliberate design of such laser 2D material interactions via the SLLC method enables the material to have a higher tolerance to process parameters in a much broader process parameter window. This method is especially important for bringing a new alternative to the future flexible nanoelectronics are a where high-performance inorganic materials, such as 2D crystals, are of interest.

REFERENCES

- [1] Coehoorn R, Haas C, Dijkstra J, Flipse C J F, Degroot R A and Wold A 1987 Electronic structure of MoSe₂, MoS₂, and WSe₂. I. Band-structure calculations and photoelectron spectroscopy Phys. Rev. B 35 6195–202

- [2] Cong CX, Shang JZ, Wu X, Cao BC, Peimyoo N, Qiu C, Sun LT and Yu T 2014 Synthesis and optical properties of large-area single-crystalline 2D semiconductor WS₂ monolayer from chemical vapor deposition *Adv. Opt. Mater.* 2131–6
- [3] Ferrer JJ, Nevskai DM, Delasheras C and Sanchez C 1990 About the band-gap nature of FeS₂ as determined from optical and photoelectrochemical measurements *Solid State Commun.* 74913–6
- [4] Gu X, Cui W, Song T, Liu CH, Shi XZ, Wang SD and Sun BQ 2014 Solution-processed 2D niobium diselenide nanosheets as efficient hole-transport layers in organic solar cells *ChemSusChem* 7416–20
- [5] Hu PA, Wen ZZ, Wang LF, Tan PH and Xiao K 2012 Synthesis of few-layer GaSe nanosheets for high performance photodetectors *ACS Nano* 65988–94
- [6] Janisch C, Wang YX, Ma D, Mehta N, Elias AL, Perea Lopez N, Terrones M, Crespi V and Liu ZW 2014 Extraordinary second harmonic generation in tungsten disulfide monolayers *Sci. Rep.* 45530
- [7] Late DJ, Liu B, Luo JJ, Yan AM, Matte HSSR, Grayson M, Rao CN and David VP 2012 GaS and GaSe ultrathin layered transistors *Adv. Mater.* 243549–54
- [8] Lei S D et al 2014 Evolution of the electronic band structure and efficient photo-detection in atomic layers of InSe *ACS Nano* 81263–72
- [9] Lopez-Sanchez O, Lembke D, Kayci M, Radenovic A and Kis A 2013 Ultra-sensitive photodetectors based on monolayer MoS₂ *Nat. Nanotechnol.* 8497–501
- [10] Mann J et al 2014 2-dimensional transition metal dichalcogenides with tunable direct bandgaps: MoS_{2(1-x)}Se_x monolayers *Adv. Mater.* 261399–404
- [11] Pradhan NR, Rhodes D, Feng SM, Xin Y, Memaran S, Moon BH, Terrones H, Terrones M and Balicas L 2014 Field-effect transistors based on few-layered α -MoTe₂ *ACS Nano* 85911–20
- [12] Pradhan NR, Rhodes D, Xin Y, Memaran S, Bhaskaran L, Siddiq M, Hillis, Ajayan P and Balicas L 2014 Ambipolar molybdenum diselenide field-effect transistors: field-effect and Hall mobilities *ACS Nano* 87923–9
- [13] Sathe DJ, Chate PA, Hankare PP, Manikshete AH and Aswar AS 2013 A novel route for synthesis, characterization of molybdenum diselenide thin films and their photovoltaic applications *J. Mater. Sci. - Mater. Electron.* 24438–42
- [14] Tamalampudi SR, Lu YY, Kumar UR, Sankar R, Liao CD, Moorthy BK, Cheng CH, Chou FC and Chen YT 2014 High performance and bendable few-layered InSe photodetectors with broad spectral response *Nano Lett.* 142800–6
- [15] Wickramaratne D, Zahid F and Lake RK 2014 Electronic and thermoelectric properties of few-layer transition metal dichalcogenides *J. Chem. Phys.* 140124710
- [16] Britnell L et al 2013 Strong light-matter interactions in heterostructures of atomically thin films *Science* 3401311–4
- [17] Lu JP, Liu HW, Tok ES and Sow CH 2016 Interactions between lasers and two-dimensional transition metal dichalcogenides *Chem. Soc. Rev.* 452494–515
- [18] Mak KF, He KL, Shan J and Heinz TF 2012 Control of valley polarization in monolayer MoS₂ by optical helicity *Nat. Nanotechnol.* 7494–8
- [19] Radisavljevic B, Radenovic A, Brivio J, Giacometti V and Kis A 2011 Single-layer MoS₂ transistors *Nat. Nanotechnol.* 6147–50
- [20] Grosso G 2017 2D materials valley polaritons *Nat. Photon.* 11455–6
- [21] Koperski M, Molas MR, Arora A, Nogajewski K, Slobodeniuk AO, Faugeras C and Potemski M 2017 Optical properties of atomically thin transition metal dichalcogenide: observations and puzzles *Nanophotonics* 61289–308
- [22] Mak KF and Shan J 2016 Photonics and optoelectronics of 2D semiconductor transition metal dichalcogenides *Nat. Photon.* 10216–26
- [23] Xia FN, Wang H, Xiao D, Dubey M and Ramasubramanian A 2014 Two-dimensional material *Nanophotonics* *Nat. Photon.* 8899–907
- [24] Mak KF, Lee C, Hone J, Shan J and Heinz TF 2010 Atomically thin MoS₂: a new direct gap semiconductor *Phys. Rev. Lett.* 105136805
- [25] Zhang Y et al 2014 Direct observation of the transition from indirect to direct band gap in atomically thin epitaxial Se₂ *Nat. Nanotechnol.* 9111–5
- [26] Ross J et al 2013 Electrical control of neutral and charged excitons in a monolayer semiconductor *Nat. Commun.* 41474
- [27] Mak KF, He KL, Lee C, Lee GH, Hone J, Heinz TF and Shan J 2013 Tightly bound trions in monolayer MoS₂ *Nat. Mater.* 12207–11
- [28] Xu XD, Yao W, Xiao D and Heinz TF 2014 Spin and pseudospins in layered transition metal dichalcogenides *Nat. Phys.* 10343–50
- [29] Chegwidden S, Dai ZR, Olmstead MA and Ohuchi FS 1998 Molecular beam epitaxy and interfacial reactions of layered GaSe growth on sapphire (0001) *J. Vac. Sci. Technol. A* 162376–80
- [30] Lee Y H et al 2012 Synthesis of large-area MoS₂ atomic layers with chemical vapor deposition *Adv. Mater.* 242320–5
- [31] Lei S D, Ge L H, Liu Z, Najmaei S, Shi G, You G, Lou J, Vajtai R and Ajayan P M 2013 Synthesis and photoresponse of large GaSe atomic layers *Nano Lett.* 132777–81
- [32] Li X F et al 2014 Controlled vapor phase growth of single crystalline, two-dimensional gas crystals with high photoresponse *Sci. Rep.* 45497
- [33] Mahjouri Samani M et al 2014 Digital transfer growth of patterned 2D metal chalcogenides by confined nanoparticle evaporation *ACS Nano* 811567–75
- [34] Shim GW, Yoo K, Seo SB, Shin J, Jung DY, Kang IS, Ahn CW, Cho BJ and Choi SY 2014 Large-area single layer MoSe₂ and its van der Waals heterostructures *ACS Nano* 86655–62
- [35] Xia J, Huang X, Liu LZ, Wang M, Wang L, Huang B, Zhu DD, Li JJ, Gu CZ and Meng XM 2014 CVD synthesis of large-area, highly crystalline MoSe₂ atomic layers on diverse substrates and application to photodetectors *Nanoscale* 68949–55
- [36] Shi YM, Li H N and Li J J 2015 Recent advances in controlled synthesis of two-dimensional transition metal dichalcogenides via vapor deposition techniques *Chem. Soc. Rev.* 442744–56
- [37] Kang K, Xie SE, Huang L J, Han Y M, Huang P Y, Mak K F, Kim CJ, Muller D and Park J 2015 High mobility three-atom-thick semiconducting films with wafer-scale homogeneity *Nature* 520656–60
- [38] Yue R Y et al 2015 HfSe₂ thin films: 2D transition metal dichalcogenides grown by molecular beam epitaxy *ACS Nano* 9474–80
- [39] Mahjouri Samani M et al 2014 Pulsed laser deposition of photoresponsive two-dimensional GaSe nanosheet networks *Adv. Funct. Mater.* 246365–71
- [40] Mahjouri Samani M et al 2017 Nonequilibrium synthesis of TiO₂ nanoparticle 'building blocks' for crystal growth by sequential attachment in pulsed laser deposition *Nano Lett.* 174624–33
- [41] Najmaei S, Yuan JT, Zhang J, Ajayan P and Lou J 2015 Synthesis and defect investigation of two-dimensional molybdenum disulfide atomic layers *Acc. Chem. Res.* 4831–40
- [42] Li H, Zhang Q, Yap CCR, Tay BK, Edwin THT, Olivier A and Baillargeat D 2012 From bulk to monolayer MoS₂: evolution of Raman scattering *Adv. Funct. Mater.* 221385–90